CME SAM

Cardiac MRI

AJR FOCUS ON:

Cardiac MRI: Part 1, Cardiovascular Shunts

Prabhakar Rajiah[1]
Jeffrey P. Kanne[2]

OBJECTIVE. MRI plays an important role in the morphologic and functional evaluation of cardiovascular shunts. Good spatiotemporal resolution, inherent contrast resolution, wide FOV, and multiplanar imaging capabilities make MRI an ideal tool in the investigation of cardiovascular shunts. The velocity-encoded phase-contrast sequence is used in the quantification of a shunt and the steady-state free precession (SSFP) sequence is used in the assessment of the functional impact of a shunt. In this article, the role of MRI in the evaluation of cardiovascular shunts and their respective MRI appearances are described and illustrated.

CONCLUSION. MRI can identify and characterize septal defects, quantify shunts and their impact on cardiac function, and help in the selection of appropriate candidates for percutaneous device placement.

Keywords: atrial septal defect, hemodynamics, MRI, shunts, ventricular septal defect

DOI:10.2214/AJR.10.7257

Received April 26, 2010; accepted after revision December 27, 2010.

[1]Imaging Institute, Cleveland Clinic, 9500 Euclid Ave, Cleveland, OH 44195. Address correspondence to P. Rajiah (radprabhakar@gmail.com).

[2]Department of Radiology, University of Wisconsin School of Medicine and Public Health, 660 Highland Ave, MC 3252, Madison, WI 53792.

SAM/CME
This article is available for SAM/CME credit.
See www.arrs.org for more information.

WEB
This is a Web exclusive article.

AJR 2011; 197:W603–W620

0361–803X/11/1974–W603

Cardiovascular shunts are abnormal communications between the systemic circulation and pulmonary circulation. In a left-to-right shunt, blood is shunted from the left side of the heart (systemic circulation) to the right side of the heart (pulmonary circulation). In a right-to-left shunt, blood is shunted from the right side of the heart (pulmonary circulation) to the left side of the heart (systemic circulation). Shunts are quantified by measuring the ratio of pulmonary blood flow (Qp) to systemic blood flow (Qs)—that is, Qp:Qs. The extent of a shunt is determined by the size of the defect and the left-to-right pressure gradient. In small left-to-right shunts (i.e., Qp:Qs < 1.5:1), the cardiac chambers are not significantly enlarged and the pulmonary vasculature is usually normal. With large shunts (Qp:Qs > 2.0:1), left atrial and left ventricular volume overload develop along with elevated right ventricular pressure and pulmonary arterial hypertension; these changes ultimately result in reversal of the shunt direction, which is called Eisenmenger syndrome [1, 2].

MRI is an excellent noninvasive imaging technique for evaluating cardiovascular shunts because of its high inherent contrast resolution, good spatiotemporal resolution, large FOV, and multiplanar imaging capabilities. MRI can accurately quantify shunts, detect associated anomalies, evaluate the pulmonary vasculature, and quantify ventricular sizes and function [1]. MRI can detect peripheral branch pulmonary arteries and systemic or pulmonary venous anomalies, which are less well seen and are often occult on echocardiography. MRI is particularly useful in patients who have an echocardiographic diagnosis of isolated right ventricular enlargement because MRI is able to depict causes such as a sinus venosus defect or partial anomalous pulmonary venous drainage before making a diagnosis of right ventricular cardiomyopathy or primary pulmonary hypertension [2].

MRI is generally not appropriate in patients with electronic cardiac devices. Anxiety and claustrophobia may require sedation. IV contrast material should be avoided in patients with moderate-to-severe renal dysfunction (estimated glomerular filtration rate < 30 mL/min) because of the risk of nephrogenic systemic fibrosis.

MRI Technique

There are various types of cardiac shunts (Table 1). A typical MRI protocol for imaging a cardiovascular shunt includes black blood images, steady-state free precession (SSFP) images, velocity-encoded phase-contrast images, MR angiography (MRA) images, and 3D whole-heart SSFP images (Table 2). Morphologic evaluation is performed using T1- or T2-weighted double inversion recovery–prepared black blood sequences. SSFP cine images are used in the evaluation of cardiac

function and quantification of ventricular volumes and masses. Velocity-encoded phase-contrast MRI is used for the quantification of vascular flow. MRA with a 3D T1-weighted spoiled gradient-echo sequence is used to define extracardiac vascular structures and anomalies with high resolution, speed, and signal-to-noise ratio and a large FOV. It is particularly useful in the detection of associated pulmonary and systemic venous anomalies. Dynamic contrast-enhanced imaging enables visualization of early and late enhancing structures.

Postprocessing techniques, including multiplanar reformations, enable evaluation of tortuous vessels and detection of stenosis. In addition, MRA often provides information that guides clinical management and also reduces the radiation in subsequent cardiac catheterization [3]. Unenhanced whole-heart 3D SSFP imaging is an effective alternative or adjunct to MRA for the delineation of vascular anatomy, cardiovascular morphology, and coronary artery origins.

Children unable to cooperate with breath-hold instructions are scanned while under general anesthesia or using free-breathing techniques such as 3D whole-heart SSFP, phase-contrast MRA, and time-of-flight MRA. Time-of-flight MRA (inflow MRA) is acquired in early diastole, the cardiac phase with maximal venous flow, to make it easier to detect venous anomalies [4].

Shunt Quantification

MRI shunt quantification can be indirect or direct. Indirect quantification can be performed using velocity-encoded phase-contrast MRI or volumetric analysis of short-axis images. Velocity-encoded phase-contrast MR images acquired perpendicular to the ascending aorta and main pulmonary artery measure aortic (Qs) and pulmonary (Qp) flows, respectively, which can be used to accurately calculate shunt volume and shunt fraction (Qp / Qs) [5] (Figs. 1A and 1B) in both adult and pediatric patients. However, this technique is not accurate when the shunt fraction is low or when there are significant valvular regurgitations. In volumetric analysis, shunt volume and shunt fraction are measured as the difference between left ventricular and right ventricular stroke volumes (Figs. 1C and 1D). However, these measurements are inaccurate in the presence of valvular regurgitations and when quantifying ventricular septal defects (VSDs), which may have equal stroke volumes [1].

Direct shunt quantification is performed using *en face* phase-contrast MRI of the septal defect [6] particularly in patients with secundum defects. Orthogonal images of the atrial septum in short-axis and four-chamber views acquired in end-systole are used to obtain double oblique through-plane *en face* phase-contrast MR images of the defect. Obtaining images during end-systole maximizes atrial septal defect (ASD) flow and minimizes errors due to septal motion. Encoded velocity is low (50–70 cm/s) so that low-velocity flow is not missed and small defects are identified. The TE is low (3 ms) to minimize phase errors. Subsequently, in-plane phase-contrast MR images are acquired in new four-chamber and short-axis views centered on the defect. Using these two images, a final double oblique through-plane phase-contrast MR image is obtained that is less foreshortened.

En face imaging provides accurate, better, and sharper definition of borders and allows accurate estimation of even small shunts [7]. The Qp:Qs ratio obtained using Qs (i.e. [Qs + Qsd] / Qs, where Qsd is flow through the septal defect) correlates better with pulse oximetry than Qp:Qs ratio obtained using Qp (i.e., Qp/[Qp – Qsd]) [6]. The Qp:Qs ratio is also

TABLE 1: Classification of Various Cardiovascular Shunts

Location	Subtype
Left-to-right shunts	
Atrial	Ostium primum
	Ostium secundum
	Sinus venosus
	Unroofed coronary sinus
Ventricular	Membranous
	Muscular
	Inlet
	Outlet
Arterial	Patent ductus arteriosus
	Aortopulmonary window defect
	Aortopulmonary collaterals
	Surgical aortopulmonary shunts
	Coronary arteriovenous fistula
	Anomalous origin of the coronary artery from the pulmonary artery
	Aorta–right atrium shunt
	Bypass graft–cardiac vein fistula
	Systemic arteriovenous shunts
Venous	Partial or total anomalous pulmonary venous drainage
Right-to-left shunts	
Atrial	Patent foramen ovale
	Tricuspid atresia
Atrial or ventricular	Tetralogy of Fallot
	Pulmonary atresia
	Transposition of great arteries
	Truncus arteriosus
	Hypoplastic left heart syndrome
Arterial	Pulmonary arteriovenous fistula or malformation
Reversal of left-to-right shunt	Atrial
	Ventricular
	Arterial
	Venous
Venous	Systemic-to-pulmonary vein communication

TABLE 2: MRI Sequences and Planes Used in Evaluation of Cardiac Shunts

Sequence	Planes	Information
Scouts	Transverse, sagittal, coronal	Localizing
HASTE	Transverse	Define anatomy, plan for subsequent views
Cine steady-state free precession	Vertical long axis, three chamber, short-axis stacks, four-chamber stacks	Evaluate function, volumes, mass
Velocity-encoded phase-contrast		
Velocity encoding = 200 cm/s	Ascending aorta, main pulmonary artery	Assess flow and estimate Qp:Qs
Velocity encoding = 50 cm/s, en face	Orthogonal to septal defect	Assess shunt volume
MR angiography	Coronal	Evaluate vasculature, detect anomalous drainage
3D Whole-heart[a] SSFP	Transverse	Assess cardiovascular anatomy, detect anomalous drainage, assess coronary artery anatomy

Note—Qp:Qs = pulmonary-to-systemic flow ratio.
[a]This is also a good sequence to use in patients with renal dysfunction who cannot receive IV contrast material.

used for precise measurement of the defect. Detection of complex defects (multiple defects, eccentric shape, atypical location) and of associated anomalies alters management. If no flow is identified on the first through-plane image, three double oblique images of the fossa ovalis should be acquired on either side of the interatrial septum before concluding that no septal defect is present [6].

Pulmonary vascular resistance (PVR) is an important parameter that needs to be assessed in patients with unrestricted left-to-right shunts who are at risk of obstructive pulmonary vascular disease. Surgery is avoided in patients with high PVR because of increased perioperative mortality. This information is typically acquired using oximetry or cardiac catheterization, both of which have limitations. Because there is an inverse exponential relationship between pulmonary blood flow (Qp) and PVR, pulmonary flow (Qp) measured with phase-contrast MRI can potentially be used to indirectly estimate the PVR [7].

Atrial Septal Defects

ASD is the second most common congenital heart disease in adults (20–40%) and accounts for 10% of congenital heart diseases overall [1, 8]. ASDs are traditionally classified as ostium secundum, ostium primum, sinus venosus, or coronary sinus defects [9]. Patients with small defects (< 1 cm) are usually asymptomatic. Hemodynamically significant shunts are those with Qp:Qs > 1.5:1 and significant right ventricular dilatation [10]. These patients may present with symptoms of heart failure, atrial arrhythmias, complete heart block, or pulmonary hypertension. The morphology of an ASD is highly variable and can be circular, oval, or complex. Multiple defects or septal aneurysms also occur. ASDs are repaired to prevent the development of pulmonary hypertension and subsequent right-to-left shunting.

Ostium Secundum Defect

Ostium secundum is the most common type of ASD (50–70%) and accounts for 40% of congenital heart diseases presenting in adults [9]. Ostium secundum is seen in the mid atrial septum at the level of fossa ovalis (Figs. 2 and S2C [Fig. S2C, a cine loop, can be viewed from the online version of this article at www.ajronline.org.]) and results from the failure of the septum secundum to close the ostium secundum because of excessive resorption of the septum primum. Ostium secundum defect is more common in females. The size of the defect is variable and can vary in different phases of the cardiac cycle; the defect is maximal in ventricular end-systole and minimal in diastole [11]. Multiple defects are seen if there is fenestration of the floor of fossa ovalis. Secundum defects can occur in isolation or as part of a syndrome such as Holt-Oram syndrome, Noonan syndrome, Treacher Collins syndrome, and thrombocytopenia–absent radius syndrome. Secundum defects may also be associated with other types of ASDs or functional mitral valve prolapse [12]. Phase-contrast MRI has been shown to accurately estimate the defect size and shape (Fig. 3) in addition to estimating shunt volume [13].

Ostium Primum Defect

Ostium primum defect (i.e., partial atrioventricular septal defect) accounts for 15–30% of ASDs. It is located in the inferobasal part of the atrial septum (Fig. 4) adjacent to the atrioventricular valves because the septum primum failed to fuse with the endocardial cushion [9]. Ostium primum defect is seen in 15% of patients with Down syndrome [10]. Compared with secundum defect, ostium primum defect is typically larger and presents at a younger age with symptoms. Inlet VSD, an atrioventricular canal defect, and cleft mitral valve are known associations. Development of symptoms and development of high-volume shunts are indications for surgical closure with a pericardial or polyester fiber (Dacron, DuPont) patch. Associated congenital abnormalities such as cleft mitral valve are generally repaired simultaneously.

Sinus Venosus Defect

Sinus venosus defect accounts for 5–10% of ASDs and is caused by a defect in the wall that normally separates the superior vena cava (SVC) or inferior vena cava (IVC) from the left atrium. The defect is located outside the fossa ovalis, at the mouth of the overriding vein.

Superior sinus venosus defect is more common than the inferior sinus venosus defect and is located immediately caudad to the orifice of the SVC (Fig. 5A), rostral and posterior to the fossa ovalis. There is a high association (85%) of partial anomalous drainage of the right superior pulmonary vein into the SVC; as a result, the quantity of left-to-right shunt in a sinus venosus defect is typically higher than in a secundum defect. This larger shunt increases the risk of pulmonary hypertension [14].

The inferior sinus venosus defect is much less common and is located at the junction of the right atrium and IVC, immediately craniad to the orifice of the IVC (Fig. 5B). It is typically associated with anomalous drainage of the right inferior pulmonary vein into the IVC.

Echocardiography can identify only 12% of these defects [2], with isolated right ventricle enlargement often being the only finding. The

diagnostic finding of caval overriding of the interatrial septum is best imaged in the transverse and sagittal planes perpendicular to the border between the left atrium and SVC (Fig. 5). The size and location of the defect can be assessed using phase-contrast MRI including *en face* views [2]. Treatment is surgical closure of the defect with a patch and baffling of the anomalous vein into the left atrium.

Coronary Sinus Defect

In coronary sinus defect (i.e., unroofed coronary sinus), there is partial or total unroofing of the septum between the coronary sinus and the left atrium, which results in a left-to-right shunt and enlargement of the coronary sinus (Fig. 6). A sizeable defect is seen in the lower part of the atrial septum near the entrance of the IVC because of enlargement of the coronary sinus orifice. A coronary sinus defect is commonly associated with a persistent left SVC which drains into the left atrium, the "Raghib" syndrome (Fig. 7) which is associated with right-to-left shunting.

In complete unroofed coronary sinus the left SVC enters the left superior corner of the left atrium, anterior to the orifice of the left superior pulmonary vein and posterior to the left atrial appendage. Cerebral thromboembolism, cerebral abscess, and pulmonary hypertension are reported complications. The partial type occurs between the left atrial appendage and left superior pulmonary vein. The defect is surgically closed with a patch (reroofing), and flow from the left SVC is redirected into the right atrium.

Patent Foramen Ovale

The foramen ovale is a flaplike opening between the septum primum and septum secundum at the level of the fossa ovalis that usually closes by the first or second year of life but that remains patent (patent foramen ovale [PFO]) in 25–30% of the population. It is not a true "defect" because septal tissue is intact and can measure up to 10 mm. In healthy individuals, shunting does not occur as long as left atrial pressure is greater than right atrial pressure and the "flap valve" remnant of the septum primum is intact. A transient right-to-left shunt can be produced by intermittent elevation of right atrial pressure in early systole, inspiration, repetitive cough or straining, and release phases of the Valsalva maneuver. In addition, a persistent fetal eustachian valve or Chiari network directs IVC flow to the midportion of the atrial septum and then into the left atrium through the defect.

At MRI, the presence of a flap- or channellike appearance of the interatrial septum and of a shunt is indicative of a PFO (Fig. 8). However, the shunt may not be evident if atrial pressures are equal during image acquisition. First-pass perfusion MRI performed at the level of the fossa ovalis with the patient performing the Valsalva maneuver can diagnose a right-to-left shunt if there is contrast flow from the right to left atrium or a contrast peak in the left atrium at the same time as in the right atrium. However, this technique detects only 63% of shunts identified on echocardiography [7, 15]. Continuous shunts are seen in 24% of patients with PFO (Fig. 8B).

An association between cryptogenic stroke and PFO exists [16], but one third of these strokes are likely incidental. Multiple studies have shown that PFO alone is not associated with a higher risk of recurrent stroke or death in patients with previous cryptogenic stroke [16]. Although a PFO can be closed percutaneously, the presence of associated partial anomalous pulmonary venous return (PAPVR) is an indication for surgical repair.

Interatrial Septal Aneurysm

Atrial septal aneurysm is redundant and mobile interatrial tissue in the region of the fossa ovalis that displaces more than 1.0–1.5 cm into either atrium (Figs. 9 and S9C). It is identified in 4% of patients undergoing transesophageal echocardiography [17] and is usually accompanied by a PFO (33%) or an ASD (19%). Intracardiac shunting occurs in up to 78% of patients with atrial septal aneurysm [17]. Atrial septal aneurysm is seen in 37% of patients with a PFO on MRI [15]. Maximal oscillation of the atrial septal aneurysm occurs just after release of the Valsalva maneuver and may be difficult to capture on cine MRI because of low temporal resolution and on real-time imaging sequences because of low spatial resolution. Although the combination of PFO and atrial septal aneurysm has previously been linked to an increased risk of subsequent stroke [16], two recent prospective studies failed to identify such as risk [18, 19].

Treatment of Atrial Septal Defects

ASDs are usually closed surgically. Seventy percent of secundum defects can also be closed percutaneously with catheter-based occluder devices [4]. Factors determining whether an ASD can be closed percutaneously include the type, location, size, and shape of the ASD and rim lengths. *En face* phase-contrast MR images of the defect (Fig. 3) are superior for precise measurement of the defect size and shape as compared with other sequences. Additional images can be acquired from the defect toward the SVC, IVC, aortic root, and atrioventricular valves to measure the lengths of rims from the edge of the ASD to the tricuspid valve (anteroinferior rim), aortic valve (anterosuperior rim), SVC (posterosuperior rim), and IVC (posteroinferior rim) [4].

Percutaneous closure is contraindicated for ASDs larger than 36 mm or rim deficiency of less than 3 mm [20]. Other relative contraindications include small atrial capacity limiting full expansion of disks; floppy septum causing prolapse of the occluder device; thin septum leading to easy tearing; and large ASD, which can be underestimated resulting in device dislodgement. After device placement, MRI can be used to assess the position of the device, identify residual shunting, and detect complications such as cardiac perforation and device embolization (Fig. 10).

Ventricular Septal Defects

VSD is the overall second most common congenital cardiac disease (20%) [1] and is often associated with other congenital cardiac anomalies, such as tetralogy of Fallot, transposition of the great arteries, atrioventricular canal, and a single ventricle. VSD may also be acquired after acute myocardial infarction, chest trauma, cardiac interventions, or endocarditis. VSDs can occur in the membranous, muscular, outlet, or inlet portions of the interventricular septum. The left atrium and left ventricle are dilated. Approximately half of VSDs are small, and half of these spontaneously close. Surgical repair is performed during infancy to prevent development of persistent pulmonary hypertension [6]. MRI can be used after treatment to assess the integrity of the patch and identify any residual shunt (Figs. 11 and S11D).

Membranous Defect

A membranous defect is the most common type of VSD (75–80%) and occurs in the upper part of the ventricular septum immediately under the aortic valve and behind the septal leaflet of the tricuspid valve at the intersection of the muscular, inlet, and outlet regions of the septum (Fig. 12). It may be associated with double-chambered right ventricle, subaortic ridge, Gerbode defect, or aortic coarctation. Membranous defect usually closes spontaneously by apposition of the septal leaflet of the

tricuspid valve or by prolapse of an aortic cusp into the defect [21]. Septal apposition can produce an aneurysm of the ventricular septum (Fig. 12) with residual shunting. Tricuspid and aortic regurgitation can occur because of the proximity of these valves to the defect.

Muscular Defect

A muscular defect accounts for 20% of VSDs and is located within the confines of the muscular septum, distal to the septal attachment of the tricuspid valve (Figs. 13A and S13B) [1]. Two thirds of muscular defects occur in the apical two thirds of the septum, where they can be overlooked when covered by thick trabeculations. Muscular defects are usually small, particularly in premature infants. Multiple muscular defects are more common when secondary to myocardial infarction. Multiple small defects ("Swiss cheese" septum) have the same hemodynamic effects as a single large defect (Figs. 14A and 14B). Seventy-five percent of small muscular VSDs spontaneously close by the age of 2 years because of growth and hypertrophy of surrounding muscle tissue in the septum [22]. Persistent small defects are usually benign (Fig. 14C).

Inlet Defect

An inlet defect (5% of VSDs) occurs at the cardiac crux at the junction of the mitral and tricuspid valves, posterosuperior to the tricuspid annulus (Fig. 15). It is usually a part of an atrioventricular septal defect. The chorda tendineae of the mitral and tricuspid valves may insert into the left and right ventricular surfaces of the ventricular septum, respectively. A common atrioventricular valve may be seen straddling the inlet defect, with anomalous chordal attachments to the septum or free wall of the opposite ventricular surface. These defects typically do not close spontaneously and require surgical correction.

Outlet Defect

An outlet defect (supracristal, doubly committed subarterial, subpulmonic, conal septal, or infundibular) accounts for 5–30% of VSDs and is more common in Asian individuals [23]. It is located below the aortic and pulmonic valves and connects the right ventricular outflow tract (above the level of crista supraventricularis) directly to the aorta (Figs. 16A and S16D). An outlet defect is associated with prolapse of the right coronary cusp (Fig. 16B) or noncoronary cusp of the aortic valve. This prolapse potentially restricts the functional size of the defect but may cause aortic regurgitation.

In the malalignment type of outlet defect, there is an abnormal relationship between the atrial and ventricular septa or between individual components of the ventricular septum with overriding of atrioventricular valves. Malalignment defects are typically seen in tetralogy of Fallot, truncus arteriosus, and double-outlet right ventricle. Anterior malalignment defects are present in tetralogy of Fallot, whereas posterior malalignment defects cause obstruction of the left ventricular outflow tract. On MRI, a malalignment defect can be confused with a membranous defect.

Atrioventricular Septal Defects

In an atrioventricular defect (i.e., an endocardial cushion defect), defects of the atrial ostium primum and ventricular inlet septum (Fig. 17) are associated with a common atrioventricular valve and abnormal arrangement of the valve leaflets. The various types of atrioventricular defects include a complete type (ostium primum ASD, inlet VSD, and cleft mitral and tricuspid valves); a partial type (ostium primum ASD, no interventricular shunt, normal atrioventricular valves); and a common atrium [20]. Direct shunting from the left ventricle into the right atrium may develop. In the most severe form, all four chambers communicate causing left-to-right and right-to-left shunting [1].

Gerbode Defect

A Gerbode defect is an abnormal communication between the left ventricle and right atrium. It is typically congenital but may be acquired. In the congenital type, there is a defect of the septal tricuspid leaflet and membranous septum below the level of tricuspid valve insertion, with resultant shunting of blood from the left ventricle to the right ventricle and right atrium through a cleft in the septal tricuspid leaflet. Acquired defects are seen below the level of insertion of the tricuspid valve in the interventricular septum and are caused by surgery, infective endocarditis, or myocardial infarction [24]. The right atrium, right ventricle, and left ventricle are dilated with Qp:Qs > 1.

Patent Ductus Arteriosus

The ductus arteriosus is a normal fetal communication between the proximal descending thoracic aorta (just beyond the left subclavian arterial origin) and the left pulmonary artery (just beyond the pulmonary bifurcation) that shunts pulmonary arterial blood into the aorta. The defect closes functionally soon after birth but occasionally may remain patent (patent ductus arteriosus), resulting in a shunt from the aorta to the pulmonary artery as pulmonary arterial pressures drop. Patent ductus arteriosus accounts for 10–12% of all congenital heart diseases, is more common in females, and is associated with maternal rubella during pregnancy [25]. It is an important contributor to the pulmonary circulation in patients with right ventricular outflow obstruction and to systemic circulation in patients with aortic coarctation, hypoplasia, or interruption.

On MRI, the communication between the proximal descending thoracic aorta and the left pulmonary artery can be seen (Fig. 18). The aorta may be focally dilated at the site of attachment of the ductus, and the aortic arch can be large [1]. Other associated findings of patent ductus arteriosus include enlargement of the main pulmonary artery, right and left ventricles, and left atrium and left or biventricular hypertrophy. Spontaneous closure is rare, and the defect usually requires surgical or percutaneous closure.

Aortopulmonary Window Defect

An aortopulmonary window defect is an abnormal communication between the ascending aorta and main pulmonary artery. The presence of both aortic and pulmonic valves and of an intact ventricular septum distinguishes it from truncus arteriosus. MRI shows a large communication between the ascending aorta and main pulmonary artery with shunting (Fig. 19). The pulmonary artery and left heart chambers are typically enlarged. Other associated anomalies include VSD, aortic coarctation, and patent ductus arteriosus. Aortopulmonary window defect requires surgical repair during infancy.

Aortopulmonary Collateral Vessels

Major aortopulmonary collaterals are arteries that arise from the systemic circulation—usually from the thoracic aorta (66.7%) and less commonly from branches of the aorta including the subclavian artery—and perfuse the lungs. They are typically seen in patients with pulmonary atresia and a VSD without a patent ductus arteriosus. Major aortopulmonary collaterals can be individual vessels larger than 2.5 mm or a cluster of multiple smaller vessels (< 2.5 mm). A recent study indicates that major aortopulmonary collaterals are dilated bronchial arteries [26]. They can supply either a single lobe or the entire lung (Fig. 20).

Thirty percent of major aortopulmonary collaterals drain into the right upper lobe, and 18% supply the right pulmonary artery [3]. In 25% of patients with major aortopulmonary collaterals, blood also reaches the lungs from the central pulmonary arteries. In pulmonary atresia, major aortopulmonary collaterals are used in the unifocalization procedure by interruption of their systemic supply and implantation into the pulmonary circulation.

Because the major aortopulmonary collaterals do not grow, they are prone to become occluded. If they are left untouched, they will decrease in size with the development of the pulmonary circulation after procedures to increase pulmonary blood flow [26]. MRI can identify these vessels, quantify ventricular size and function, and evaluate patients after repair including detecting residual shunt [3].

Surgical Aortopulmonary Shunts

Surgical aortopulmonary shunts increase pulmonary blood flow and reduce cyanosis in conditions such as tetralogy of Fallot with pulmonic stenosis or atresia, tricuspid atresia, pulmonary atresia, and single ventricle. The various surgical shunts include the Blalock-Taussig shunt (end-to-side anastomosis of a subclavian artery to the ipsilateral branch pulmonary artery), modified Blalock-Taussig shunt (prosthetic graft connecting a subclavian artery to an ipsilateral branch pulmonary artery), Waterston shunt (ascending aorta to right pulmonary artery), Potts shunt (descending aorta to left pulmonary artery), and a central shunt (aorta to main pulmonary artery) (Fig. 21).

Anomalous Pulmonary Venous Return

In total anomalous pulmonary venous return (TAPVR) all of the pulmonary veins drain into the right atrium or a systemic venous channel at supracardiac, cardiac, or infradiaphragmatic levels. Connections may rarely exist at more than one level. The supracardiac type most commonly involves a vertical vein that connects to the brachiocephalic vein. In the cardiac type, the anomalous vein drains directly into the right atrium or coronary sinus. The infradiaphragmatic type typically drains into the portal vein. Venous obstruction may be present.

In PAPVR, one to three pulmonary veins drain into the systemic venous circulation, either directly into the right atrium or into systemic veins, resulting in a partial left-to-right shunt. PAPVR is usually an incidental finding occurring in 0.7% of the population [27, 28]. It most commonly affects the left upper lobe (47%), draining into the left brachiocephalic vein (Fig. 22A), followed by the right upper lobe (38%) (Fig. 22B), right lower lobe (13%), and left lower lobe (2%) [27]. PAPVR is bilateral in 4% of patients. A sinus venosus ASD occurs in 42% of people with PAPVR of the right upper lobe [29]. MRI can easily identify and quantify a sinus venosus ASD and associated anomalous pulmonary veins that are otherwise occult on echocardiography. Transverse plane acquisitions and 3D MRA or 3D whole-heart SSFP sequences can depict these lesions. Flow into the right atrium can be confirmed and quantified with velocity-encoded phase-contrast MRI [2].

Scimitar syndrome (i.e., hypogenetic lung or venolobar syndrome) is characterized by anomalous drainage of part of or of the entire right lung into the IVC, coronary sinus, right atrium, azygos vein, portal vein, or hepatic vein in addition to hypoplasia of the right lung and right pulmonary artery. The anomalous pulmonary vein curves medially toward the diaphragm and the IVC, giving the characteristic appearance of a scimitar (Fig. 23).

Coronary Artery Fistula

Coronary artery fistula is an abnormal communication between the coronary artery and a chamber of the heart (i.e., coronary-cameral fistula) or any segment of the systemic or pulmonary circulation (coronary arteriovenous fistula) that bypasses the myocardial capillaries. It is rare (0.1–0.4%) and can be congenital or secondary to trauma or invasive cardiac procedures such as pacemaker implantation, radiofrequency ablation, endomyocardial biopsy, coronary angiography, or septal myectomy. The right coronary artery is more frequently involved (50%) than the left coronary artery (42%). Coronary artery fistulas are bilateral in 5% of patients. Drainage into the right heart circulation is most common (right ventricle, 41%; right atrium, 26%; pulmonary artery, 17%; coronary sinus, 7%; SVC, 1%), causing a small and usually undetectable left-to-right shunt in 90% of patients [30]. Occasionally, coronary artery fistulas drain into the left heart circulation (left atrium, 5%; left ventricle, 3%), resulting in left chamber volume overload.

Patients with small fistulas can be asymptomatic and are usually followed conservatively. Large fistulas can result in cardiac failure, myocardial ischemia and infarction, infective endocarditis, dissection, dysrhythmia, vessel rupture, or embolization necessitating percutaneous or surgical repair. MRI shows the origin and termination of abnormal vessels along with quantification of the shunt (Fig. 24).

Coronary Artery From Pulmonary Artery

Anomalous origin of left coronary artery from pulmonary artery (ALCAPA), or Bland-Garland-White syndrome, is rare (0.4%) and involves the left coronary artery more often than the left circumflex or right coronary arteries. In this condition, a portion of the myocardium is perfused by deoxygenated pulmonary artery blood. Because of the reduced pressure in the myocardium perfused by the anomalous coronary artery, coronary artery collaterals may develop, leading to the "steal" phenomenon in territories remote from the ALCAPA. The childhood mortality rate is 90%. Clinical presentation depends on the artery involved, distribution of affected myocardium, PVR, and number and sizes of collaterals. Surgical repair entails reimplantation or tunneling of the involved coronary artery to the aorta [31].

Miscellaneous Shunts

A sinus of Valsalva aneurysm can rupture into the right atrium or right ventricle and produce an immediate left-to-right shunt.

An aorta-to–right atrium fistula results from an intimal tear near the aortic root, especially in patients with previous cardiac surgery or those with infective endocarditis. High intraaortic pressure promotes progression of the tear toward the adventitia. Dense pericardial adhesions from previous surgery probably contain the rupture and contribute to formation of the aorta–right atrium fistula (Fig. 25). Coronary artery rupture is an associated complication [32].

Bypass graft–to-venous fistula is very rare, caused by inadvertent anastomosis, and is more common with venous grafts than with arterial grafts. Small shunts can be managed medically, but large shunts causing symptoms require repeat surgery or embolization of the fistula. Heart failure develops in 60% of patients and the mortality rate is 40% [33].

Conclusion

MRI is an ideal diagnostic examination for the comprehensive assessment of cardiovascular shunts. Good spatiotemporal resolution, multiplanar reconstruction capabilities,

and wide FOV allow evaluation of shunts and associated cardiac and pulmonary anomalies. MRI can identify and characterize septal defects, quantify shunts and their impact on cardiac function, and help in the selection of appropriate candidates for percutaneous device placement.

References

1. Wang ZJ, Reddy GP, Gotway MB, Yeh BM, Higgins CB. Cardiovascular shunts: MR imaging evaluation. *RadioGraphics* 2003; 23 (spec no):S181–S194
2. Kafka H, Mohiaddin RH. Cardiac MRI and pulmonary MR angiography of sinus venosus defect and partial anomalous pulmonary venous connection in cause of right undiagnosed ventricular enlargement. *AJR* 2009; 192:259–266
3. Prasad SK, Soukias N, Hornung T, et al. Role of magnetic resonance angiography in the diagnosis of major aortopulmonary collateral arteries and partial anomalous pulmonary venous drainage. *Circulation* 2004; 109:207–214
4. Beerbaum P, Korperich H, Esdom H, et al. Atrial septal defects in pediatric patients: noninvasive sizing with cardiovascular MRI. *Radiology* 2003; 228:361–369
5. Beerbaum P, Körperich H, Barth P, Esdorn H, Gieseke J, Meyer H. Noninvasive quantification of left-to-right shunt in pediatric patients: phase-contrast cine magnetic resonance imaging compared with invasive oximetry. *Circulation* 2001; 103:2476–2482
6. Thomson LE, Crowley AL, Heitner JF, et al. Direct *en face* imaging of secundum atrial septal defects by velocity-encoded cardiovascular magnetic resonance in patients evaluated for possible transcatheter closure. *Circ Cardiovasc Imaging* 2008; 1:31–40
7. Bell A, Beerbaum P, Greil G, et al. Noninvasive assessment of pulmonary artery flow and resistance by cardiac magnetic resonance in congenital heart diseases with unrestricted left-to-right shunt. *JACC Cardiovasc Imaging* 2009; 2:1285–1291
8. Feldt RH, Avasthey P, Yoshimasu F, Kurland LT, Titus JL. Incidence of congenital heart disease in children born to residents of Olmsted County, Minnesota, 1950–1969. *Mayo Clin Proc* 1971; 46: 794–799
9. Park MK. Chapter 12: left to right shunt lesions. In: Park MK, ed. *Pediatric cardiology for practitioners*, 5th ed. St. Louis, MO: Mosby, 2007:131–135
10. Hoey ET, Gopan D, Ganesh V, Agrawal SKB, Screaton NJ. Atrial septal defects: magnetic resonance imaging and computed tomography appearances. *J Med Imaging Radiat Oncol* 2009; 53:261–270
11. Ko SF, Liang CD, Yip HK, et al. Amplatzer septal occluder closure of atrial septal defect: evaluation of transthoracic echocardiography, cardiac CT, and transesophageal echocardiography. *AJR* 2009; 193:1522–1529
12. Steiner RM, Reddy GP, Flicker S. Congenital cardiovascular disease in the adult. *J Thorac Imaging* 2002; 17:1–17
13. Beerbaum P, Parish V, Bell A, Gieseke J, Körperich H, Sarikouch S. Atypical atrial septal defects in children: noninvasive evaluation by cardiac MRI. *Pediatr Radiol* 2008; 38:1188–1194
14. Vogel M, Berger F, Kramer A, Alexi-Meshkishvii V, Lange PE. Incidence of secondary pulmonary hypertension in adults with atrial or sinus venosus defects. *Heart* 1999; 82:30–33
15. Nusser T, Höher M, Merkle N, et al. Cardiac magnetic resonance imaging and transesophageal echocardiography in patients with transcatheter closure of patent foramen ovale. *J Am Coll Cardiol* 2006; 48:322–329
16. Messe SR, Silverman IE, Kizer JR, et al.; Quality Standards Subcommittee of the American Academy of Neurology. Practice parameter: recurrent stroke with patent foramen ovale and atrial septal aneurysm: report of the Quality Standards Subcommittee of the American Academy of Neurology. *Neurology* 2004; 62:1042–1050
17. Pearson AC, Nagelhout D, Castello R, Gomez CR, Labovitz AJ. Atrial septal aneurysm and stroke: a transesophageal echocardiographic study. *J Am Coll Cardiol* 1991; 18:1223–1229
18. Homma S, Sacco RL, Di Tullio MR, Sciacca RR, Mohr JP; PFO in Cryptogenic Stroke Study (PICSS) Investigators. Effect of medical treatment in stroke patients with patent foramen ovale: patent foramen ovale in Cryptogenic Stroke Study. *Circulation* 2002; 105:2625–2631
19. Serena J, Marti-Fàbregas J, Santamarina E, et al.; CODICIA; Right-to-Left Shunt in Cryptogenic Stroke Study: Stroke Project of the Cerebrovascular Diseases Study Group; Spanish Society of Neurology. Recurrent stroke and massive right-to-left shunt: results from the prospective Spanish multicenter (CODICIA) study. *Stroke* 2008; 39:3131–3136
20. Webb GD, Smallhorn JF, Therrien J, et al. Chapter 61: congenital heart diseases. In: Libby P, Bonow RO, Mann DL, et al., eds. *Braunwald's heart disease: a textbook of cardiovascular medicine*, 8th ed. St. Louis, MO: Saunders, 2007:1563–1564
21. Anderson RH, Lenox CC, Zuberbuhle JR. Mechanisms of closure of perimembranous ventricular septal defect. *Am J Cardiol* 1983; 52:341–345
22. Roguin N, Du ZD, Barak M, Nasser N, Hershkowitz S, Milgram E. High prevalence of muscular ventricular septal defect in neonates. *J Am Coll Cardiol* 1995; 26:1545–1548
23. Ando M, Takao A. Pathological anatomy of ventricular septal defect associated with aortic valve prolapse and regurgitation. *Heart Vessels* 1986; 2:117–126
24. Riemenschneider TA, Moss AJ. Left ventricular–right atrial communication. *Am J Cardiol* 1967; 19:710–718
25. Therrien J, Webb GD. Congenital heart disease in adults. In: Braunwald E, ed. *Heart disease: a textbook of cardiovascular medicine*, 6th ed. Philadelphia, PA: Saunders 2001:1592–1621
26. Nørgaard MA, Alphonso N, Cochrane AD, Menahem S, Brizard CP, d'Udekem Y. Major aortopulmonary collateral arteries of patients with pulmonary atresia and ventricular septal defect are dilated bronchial arteries. *Eur J Cardiothorac Surg* 2006; 29:653–658
27. Healey JE Jr. An anatomic survey of anomalous pulmonary veins: their clinical significance. *J Thorac Surg* 1952; 23:433
28. Ho ML, Bhalla S, Bierhals A, Gutierrez F. MDCT of partial anomalous pulmonary venous return in adults. *J Thorac Imaging* 2009; 24:89–95
29. Ho SY. Pulmonary vein ablation in atrial fibrillation: does anatomy matter? *J Cardiovasc Electrophysiol* 2003; 14:156–157
30. Zenooz NA, Habibi R, Mammen L, Finn PJ, Gilkeson RC. Coronary artery fistulas: CT findings. *RadioGraphics* 2009; 29:781–789
31. Zeina AR, Blinder J, Rosenschein U, Barmeir E. Coronary–pulmonary artery fistula diagnosed by multidetector CT. *Postgrad Med J* 2006; 82:254–261
32. Hsu RB, Chien CY, Wang SS, et al. Aorto–right atrial fistula: a rare complication of aortic dissection. *Tex Heart Inst J* 2000; 27:64–66
33. Khunnawat C, Mukerji S, Abela SS, Thakur RK. Unusual complications of coronary artery bypass graft surgery. *Am J Cardiol* 2006; 98:1665–1666

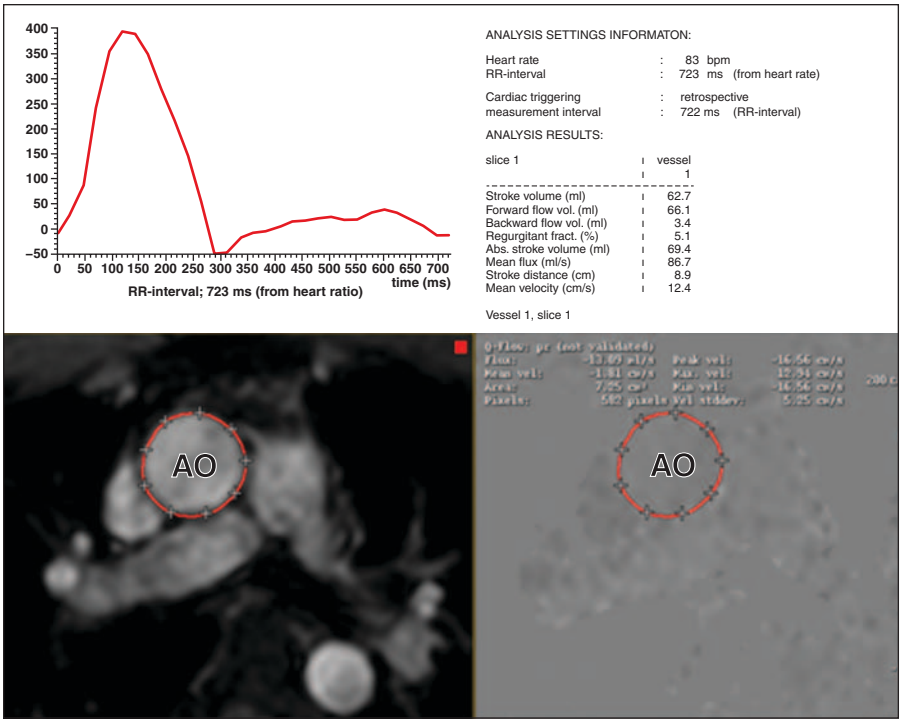

A

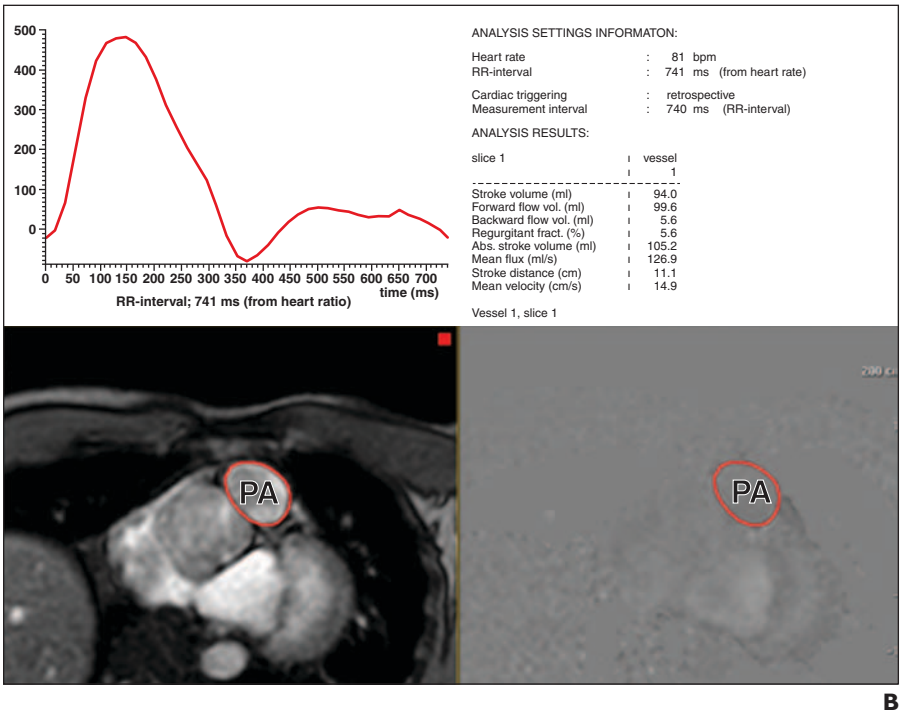

B

Fig. 1—Estimation of shunt volume and fraction in 46-year-old woman.
A, Velocity-encoded phase-contrast image acquired perpendicular to aorta (AO) is used to estimate systemic blood flow (Qs), as shown in graph.
B, Velocity-encoded phase-contrast image acquired perpendicular to main pulmonary artery (PA) is used to estimate pulmonary blood flow (Qp), as shown in graph. Qp:Qs ratio, which is an estimate of shunt fraction, can be calculated from these data.
(Fig. 1 continues on next page)

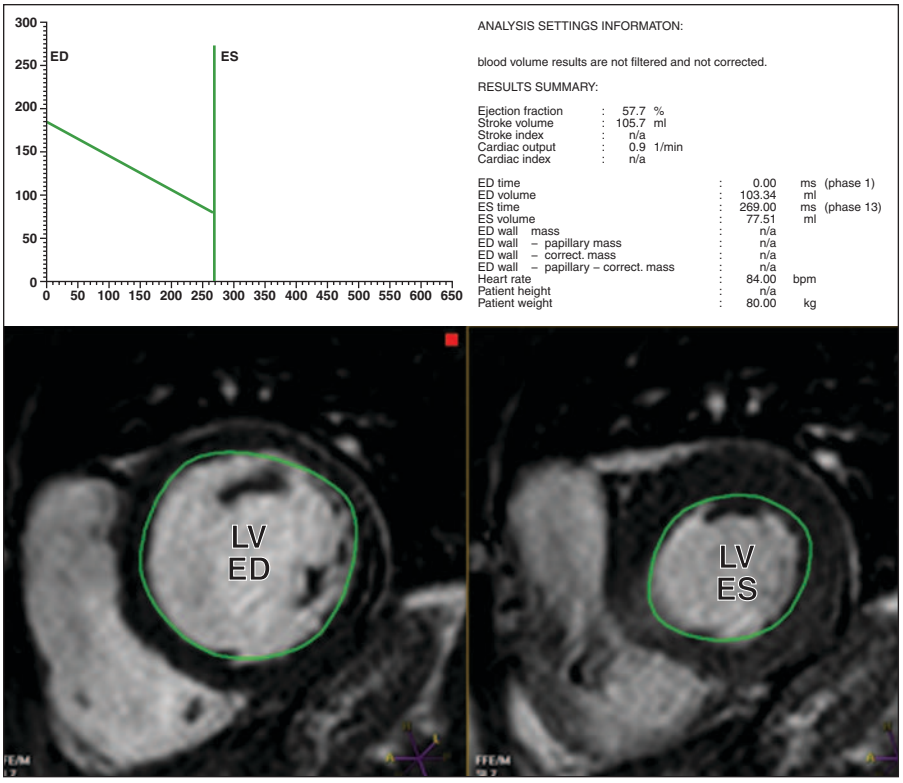

C

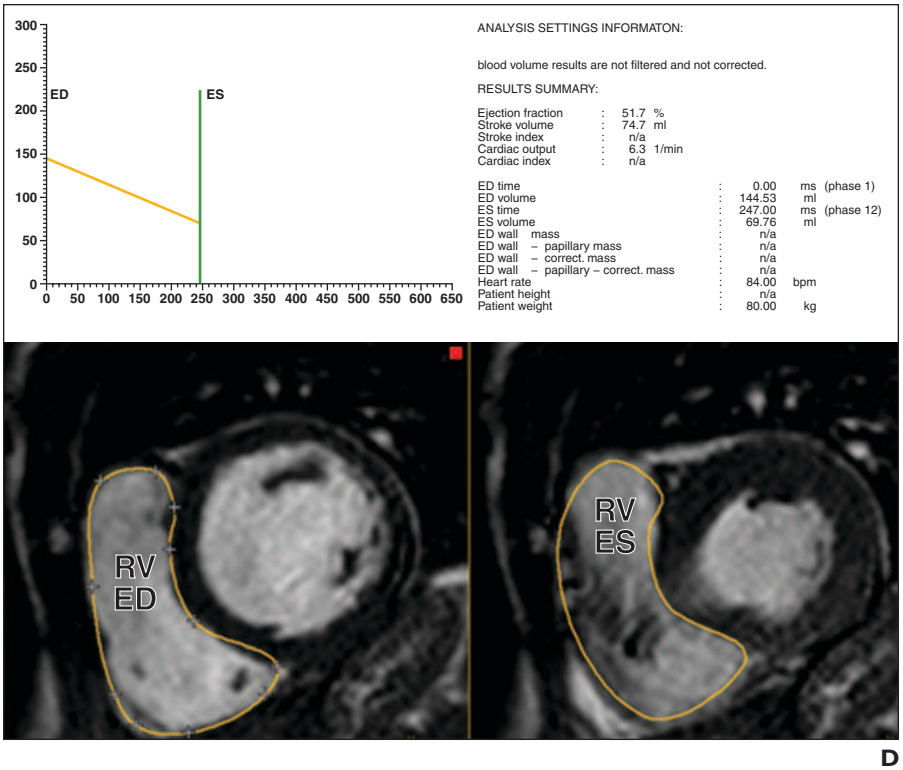

D

Fig. 1 (continued)—Estimation of shunt volume and fraction in 46-year-old woman.
C, Endocardial contour (*green*) is drawn in end-diastolic image of left ventricle (LV ED) and end-systolic image of left ventricle (LV ES), difference of which is left ventricular stroke volume.
D, Endocardial contour (*yellow*) is drawn in end-diastolic image of right ventricle (RV ED) and end-systolic image of right ventricle (RV ES), difference of which is right ventricular stroke volume. Ratio of right ventricular and left ventricular stroke volumes is estimate of shunt fraction.

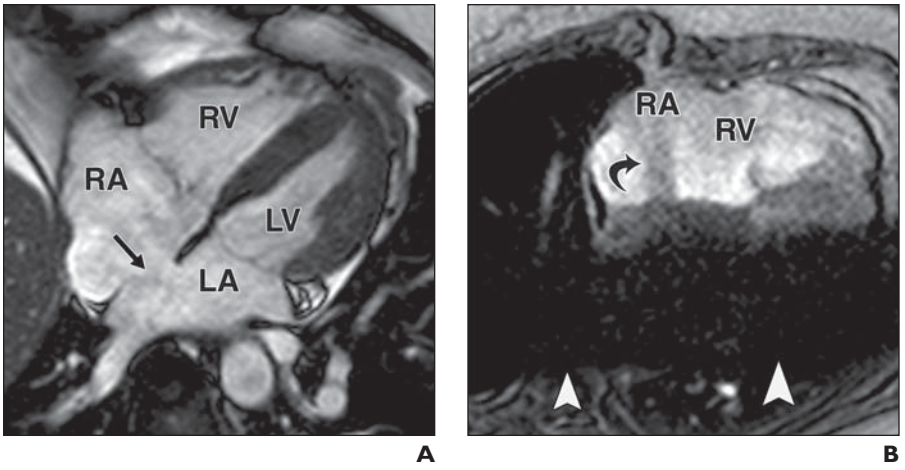

Fig. 2—Ostium secundum defect in 47-year-old man. Also, see Figure S2C, cine loop, which can be viewed from online version of this article at www.ajronline.org. RA = right atrium, RV = right ventricle, LA = left atrium, LV = left ventricle.
A, Four-chamber steady-state free precession image shows large defect (*arrow*) in region of fossa ovalis consistent with ostium secundum defect.
B, Gradient-echo image with saturation band on left side of heart (*arrowheads*). Dark jet (*arrow*) is seen extending from left to right atrium; this finding is consistent with ostium secundum defect.

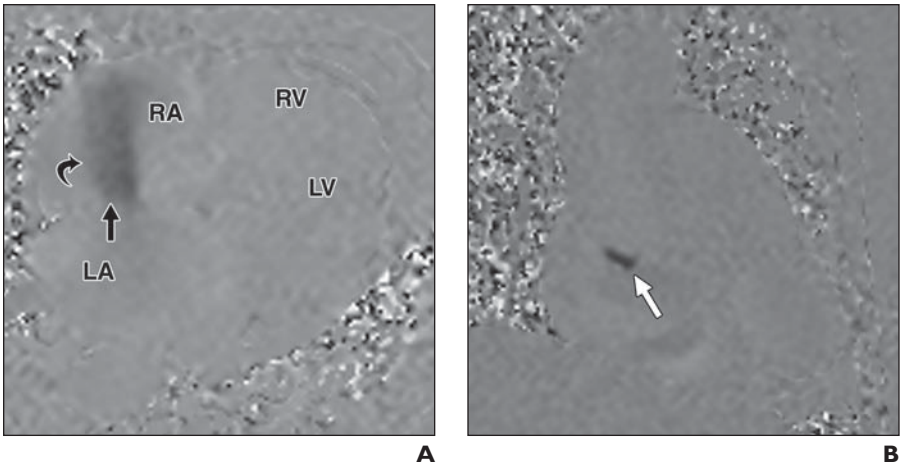

Fig. 3—38-year-old woman with ostium secundum defect.
A, Velocity-encoded phase-contrast in-plane image (velocity encoding, 50 cm/s) shows secundum defect (*straight arrow*) in mid interatrial septum, with jet (*curved arrow*) extending from left atrium (LA) to right atrium (RA). RV = right ventricle, LV = left ventricle.
B, Phase-contrast image (velocity encoding, 50 cm/s) obtained perpendicular to **A** shows jet (*arrow*) through septal defect *en face*, which is useful for precise measurement of defect and estimation of shunt volume.

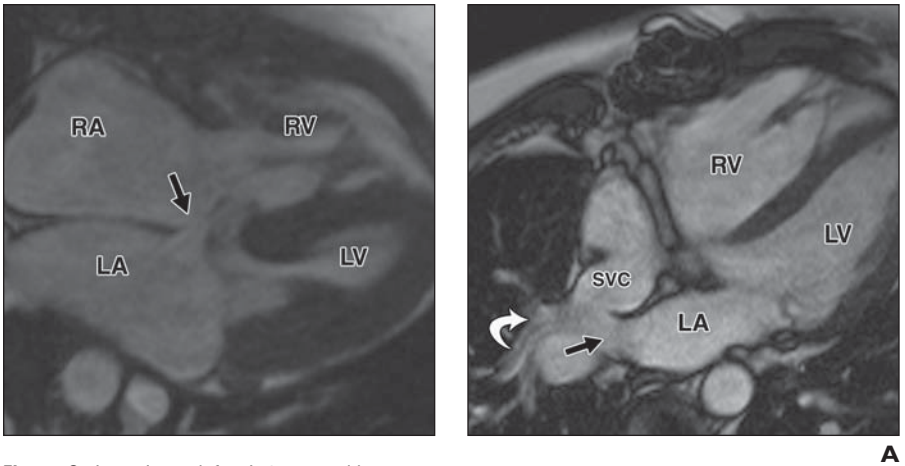

Fig. 4—Ostium primum defect in 34-year-old woman. Four-chamber steady-state free precession image shows defect in lower interatrial septum (*arrow*) consistent with ostium primum defect. RA = right atrium, RV = right ventricle, LA = left atrium, LV = left ventricle.

Fig. 5—Sinus venosus defect.
A, Axial steady-state free precession (SSFP) image of 43-year-old woman shows sinus venosus defect (*straight arrow*) between superior vena cava (SVC) and left atrium (LA). Note also anomalous right upper lobe pulmonary vein (*curved arrow*) opening into SVC. RV = right ventricle, LV = left ventricle.
B, Short-axis SSFP image of 54-year-old woman shows inferior sinus venosus defect (*straight arrow*) between inferior vena cava (IVC) and left atrium (LA), with jet (*curved arrow*) extending from LA to IVC. RA = right atrium.

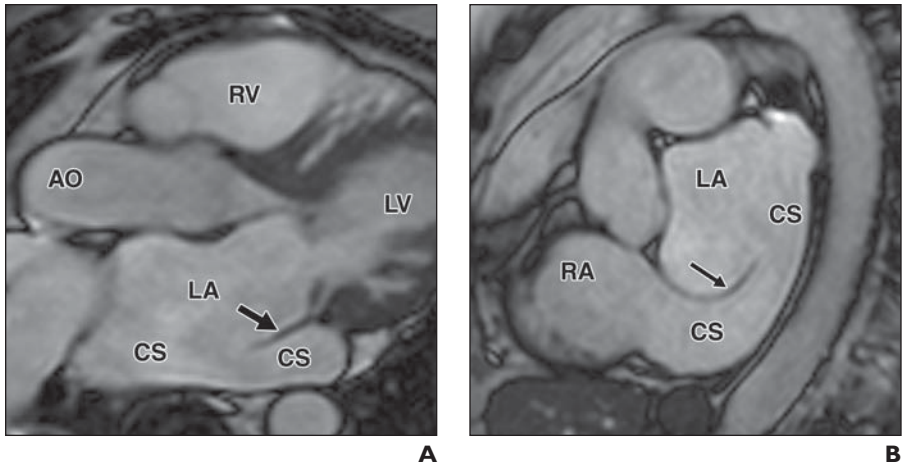

Fig. 6—Unroofed coronary sinus (CS) in 51-year-old woman.
A, Axial steady-state free precession image shows complete unroofing of coronary sinus (*arrow*) and direct communication between it and left atrium (LA). RV = right ventricle, LV = left ventricle, AO = aorta.
B, Sagittal image shows communication between coronary sinus (*arrow*) and left atrium (LA). RA = right atrium.

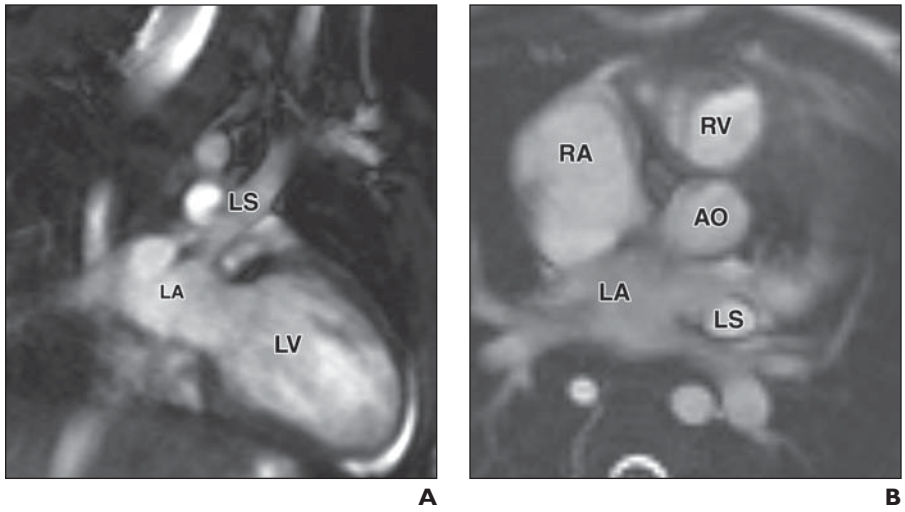

Fig. 7—Left superior vena cava (SVC) in 2-year-old girl.
A, Vertical long-axis steady-state free precession (SSFP) image shows left SVC (LS) opening into left atrium (LA). LV = left ventricle.
B, Axial SSFP image shows point of entry of left SVC (LS) into left atrium (LA). RA = right atrium, RV = right ventricle, AO = ascending aorta.

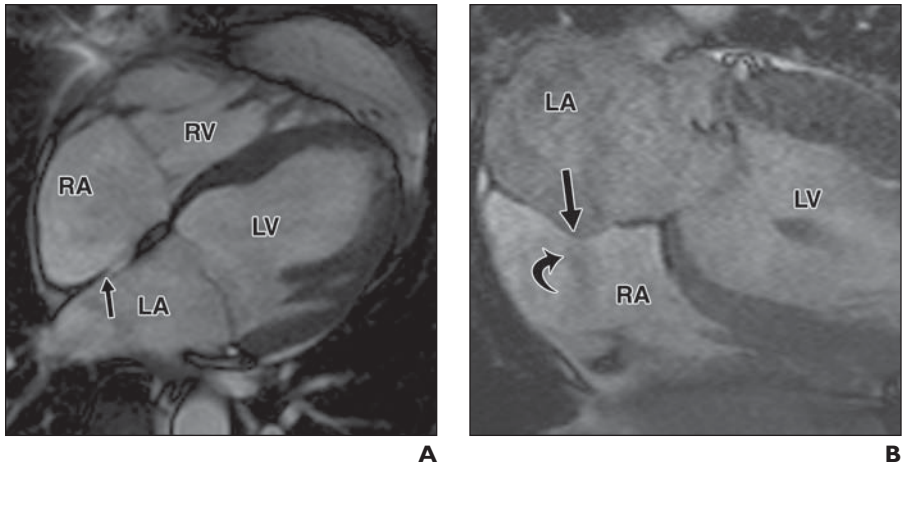

Fig. 8—Patent foramen ovale.
A, Four-chamber steady-state free precession (SSFP) image of 61-year-old woman shows patent foramen ovale (*arrow*) in midportion of interatrial septum. LA = left atrium, LV = left ventricle, RA = right atrium, RV = right ventricle.
B, Four-chamber SSFP image of 37-year-old woman shows small patent foramen ovale (*straight arrow*) with shunting of blood (*curved arrow*) from left atrium (LA) to right atrium (RA). LV = left ventricle.

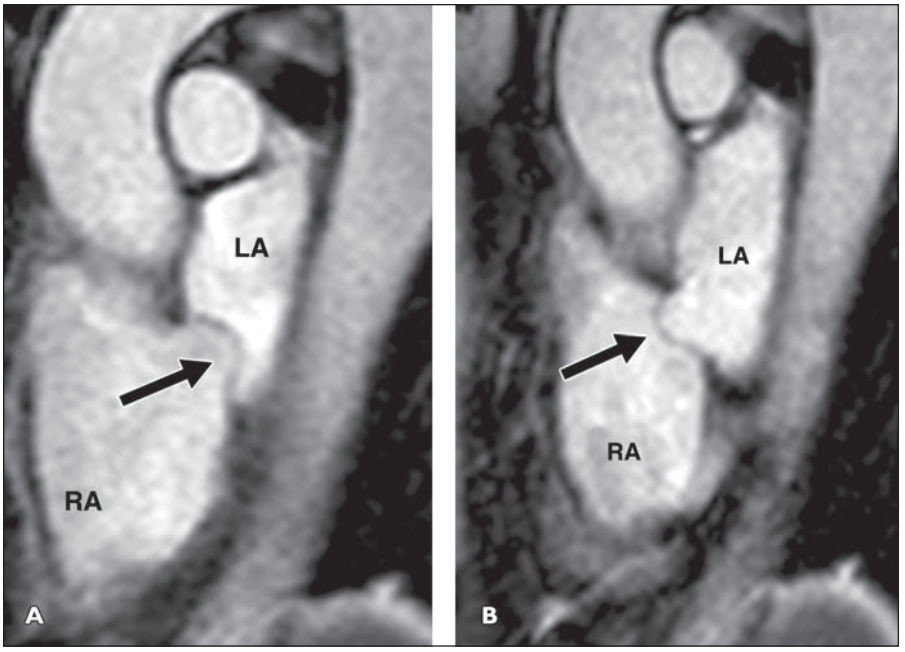

Fig. 9—Atrial septal aneurysm in 54-year-old man. Also, see Figure S9C, cine loop, which can be viewed from online version of this article at www.ajronline.org. RA = right atrium, LA = left atrium.
A, Diastolic short-axis steady-state free precession (SSFP) image of interatrial septum shows bulging of atrial septum (*arrow*) into left atrium.
B, Systolic short-axis SSFP image of interatrial septum shows bulging of atrial septum (*arrow*) into right atrium. Combined total excursion in systole and diastole is 15 mm.

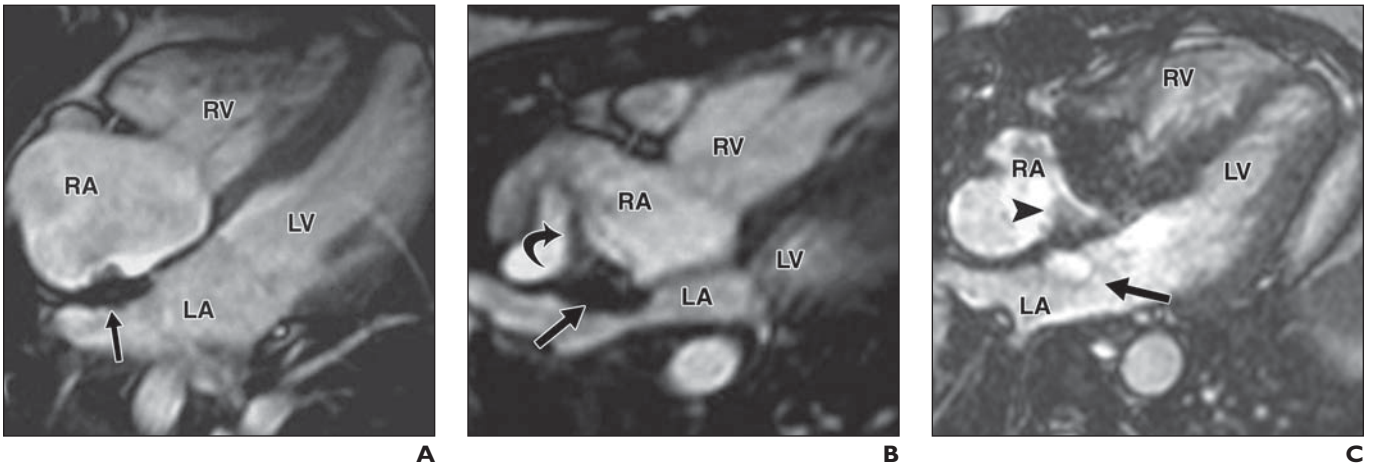

Fig. 10—Atrial septal defects (ASDs) that have been repaired. LA = left atrium, LV = left ventricle, RA = right atrium, RV = right ventricle.
A, Four-chamber steady-state free precession (SSFP) image of 42-year-old woman shows normal appearance of atrial septal occluder device (*arrow*). No residual shunt is seen.
B, Four-chamber SSFP image of 39-year-old woman shows atrial septal occluder device (*straight arrow*) and small residual left-to-right shunt (*curved arrow*).
C, Axial SSFP image obtained after patch repair of ASD in 45-year-old woman shows small contained aneurysm (*arrow*) with residual ASD (*arrowhead*).

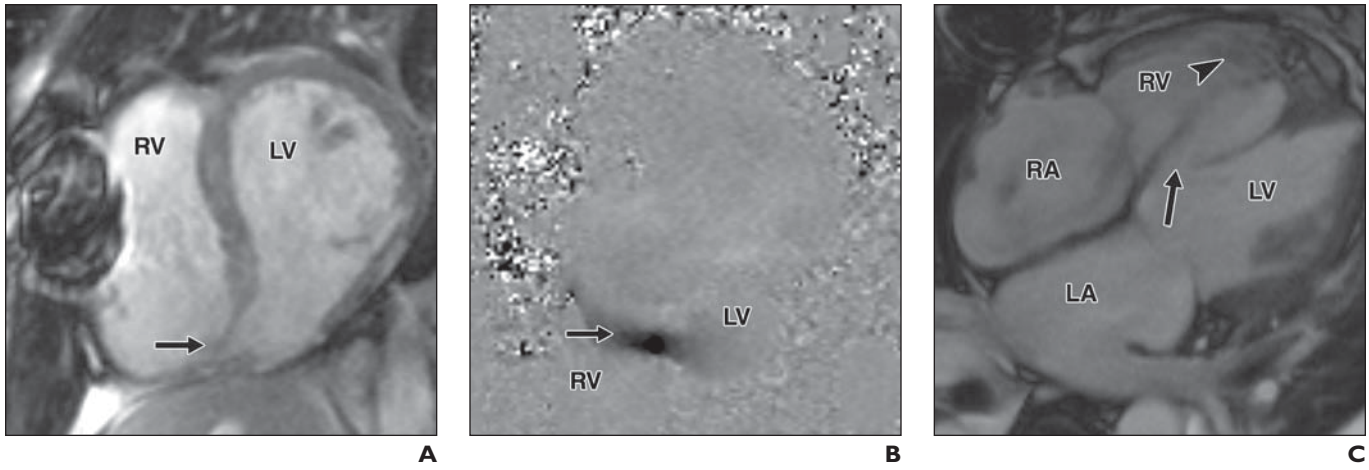

Fig. 11—Patch repairs of ventricular septal defects (VSDs). Also, see Figure S11D, cine loop, which can be viewed from online version of this article at www.ajronline.org. RV = right ventricle, LV = left ventricle, RA = right atrium, LA = left atrium.
A, Short-axis steady-state free precession (SSFP) image of 65-year-old man who had coronary artery bypass graft and patch repair for VSD that developed after myocardial infarction shows residual small defect in patch (*arrow*).
B, Phase-contrast image in short axis of same patient shown in **A** reveals shunting from left ventricle to right ventricle (*arrow*).
C, Four-chamber SSFP image of 32-year-old man with VSD patch shows dehiscence of patch (*arrow*), with left-to-right shunt directed toward right ventricular apex (*arrowhead*).

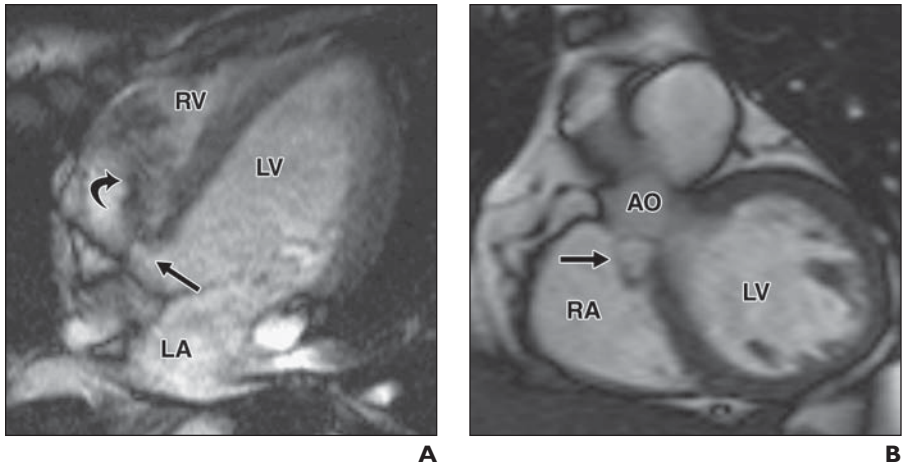

Fig. 12—Membranous septal defect in 48-year-old man. LV = left ventricle.
A, Four-chamber steady-state free precession (SSFP) image shows left-to-right shunt (*curved arrow*) through membranous ventricular septal defect (*straight arrow*). RV = right ventricle, LA = left atrium.
B, Coronal SSFP image shows aneurysm of membranous interventricular septum (*arrow*). RA = right atrium, AO = aorta.

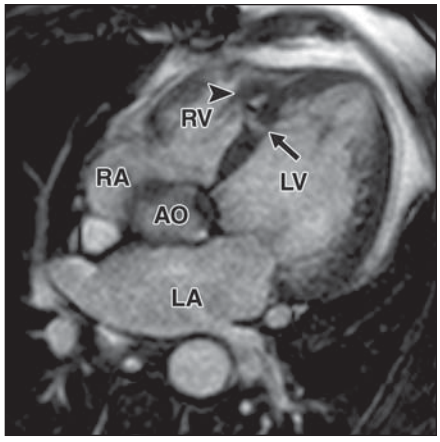

Fig. 13—Muscular defects. Also, see Figure S13B, a cine loop, which can be viewed from the information box in the upper right corner of this article. Axial steady-state free precession image of 41-year-old man shows defect (*arrow*) in muscular portion of interventricular septum, with left-to-right shunt (*arrowhead*). RV = right ventricle, LV = left ventricle, RA = right atrium, LA = left atrium, AO = aorta.

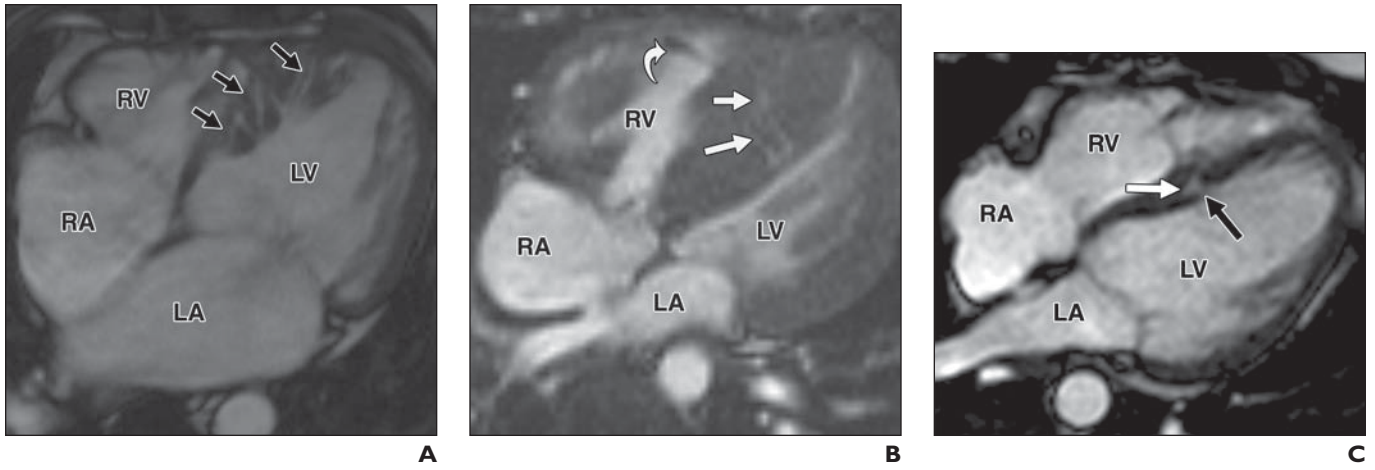

Fig. 14—Muscular defects. RV = right ventricle, LV = left ventricle, RA = right atrium, LA = left atrium.
A, Four-chamber steady-state free precession (SSFP) image of 37-year-old woman shows Swiss cheese appearance of multiple small ventricular septal defects (VSDs) (*arrows*).
B, Four-chamber SSFP image of 3-year-old boy shows serpentine defects in muscular ventricular septum (*straight arrows*) with jet of left-to-right shunt (*curved arrow*).
C, Four-chamber SSFP image of 39-year-old man shows oblique cleft (*arrows*) in midventricular septum indicative of closed VSD in midventricular septum.

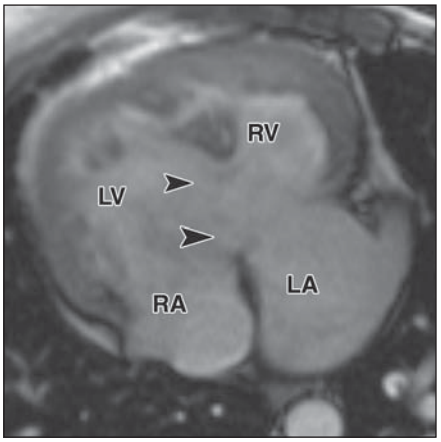

Fig. 15—Inlet defect. Four-chamber steady-state free precession image of 35-year-old man with congenitally corrected transposition of great arteries and dextrocardia shows 3.6-cm defect in inlet portion of ventricular septum (*arrowheads*). RV = right ventricle, LV = left ventricle, RA = right atrium, LA = left atrium.

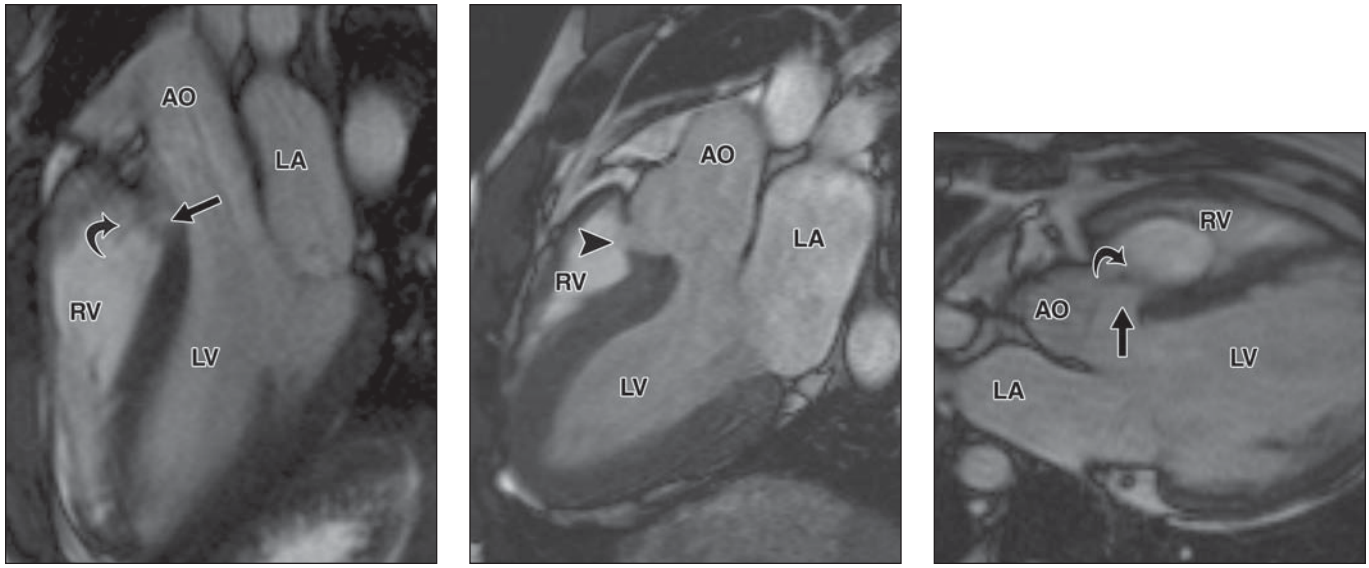

Fig. 16—Outlet defects. Also, see Figure S16D, cine loop, which can be viewed from online version of this article at www.ajronline.org. AO = aorta, LA = left atrium, RV = right ventricle, LV = left ventricle.
A, Three-chamber steady-state free precession (SSFP) image of 29-year-old man shows defect in outlet portion of ventricular septum (*straight arrow*) with jet (*curved arrow*) extending from just below aortic root to right ventricular outflow tract.
B, Three-chamber SSFP image obtained in systole at slightly inferior location relative to **A** shows prolapse of right coronary cusp into defect (*arrowhead*).
C, Horizontal long-axis SSFP image of 13-year-old girl with uncorrected tetralogy of Fallot shows malalignment type of ventricular septal defect (*straight arrow*) with left-to-right shunt (*curved arrow*). Note overriding of aorta.

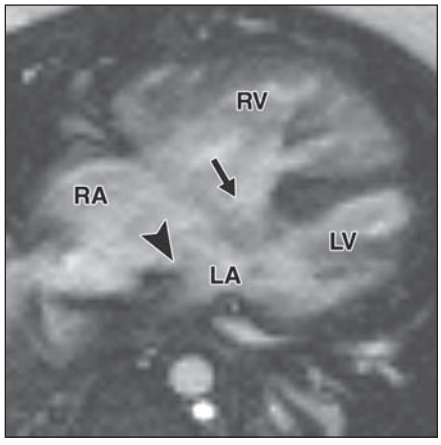

Fig. 17—Atrioventricular septal defect. Axial steady-state free precession image of 2-year-old girl shows atrioventricular septal defect with ostium primum atrial septal defect (*arrowhead*) and inlet ventricular septal defect (*arrow*). RV = right ventricle, LV = left ventricle, RA = right atrium, LA = left atrium.

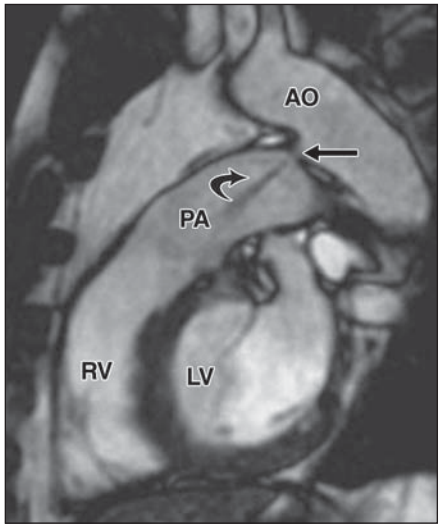

Fig. 18—Patent ductus arteriosus. Sagittal steady-state free precession image of 32-year-old man shows patent ductus arteriosus (*straight arrow*) connecting aortic isthmus with main pulmonary artery (PA), with high-velocity jet (*curved arrow*) present throughout cardiac cycle. RV = right ventricle, LV = left ventricle, AO = aorta.

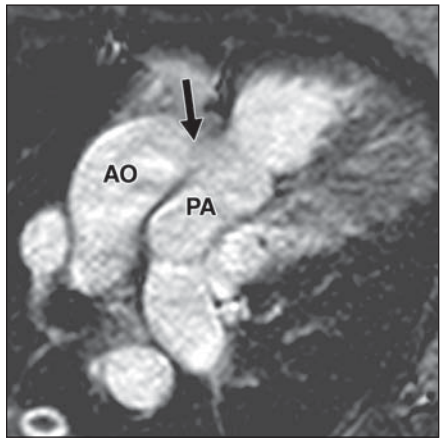

Fig. 19—Aortopulmonary window defect. Axial steady-state free precession image of 27-year-old woman shows communication (*arrow*) between aorta (AO) and main pulmonary artery (PA) consistent with aortopulmonary window defect.

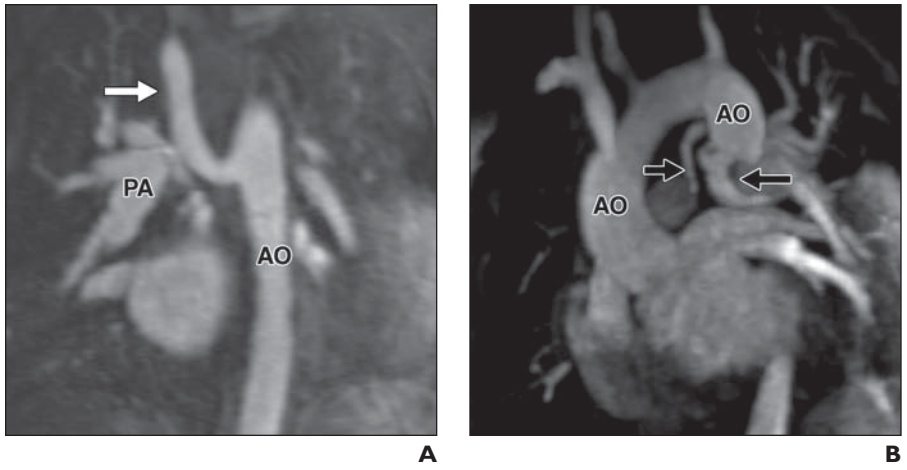

Fig. 20—Aortopulmonary collateral in 36-year-old man with repaired tetralogy of Fallot.
A, Coronal reconstructed MR angiography (MRA) image shows large collateral vessel (*arrow*) originating from proximal descending thoracic aorta (AO) and extending to right upper lobe. PA = pulmonary artery.
B, Sagittal oblique reconstructed MRA image shows another aortopulmonary collateral vessel (*arrows*) originating from descending thoracic aorta (AO) and extending to left lung.

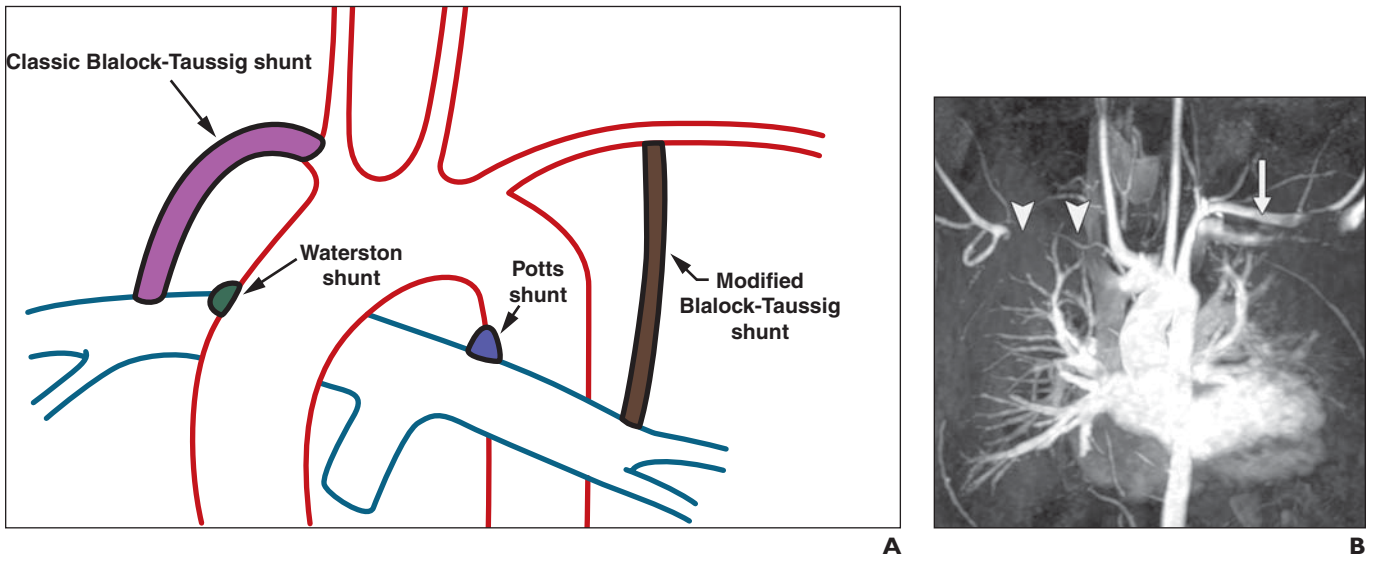

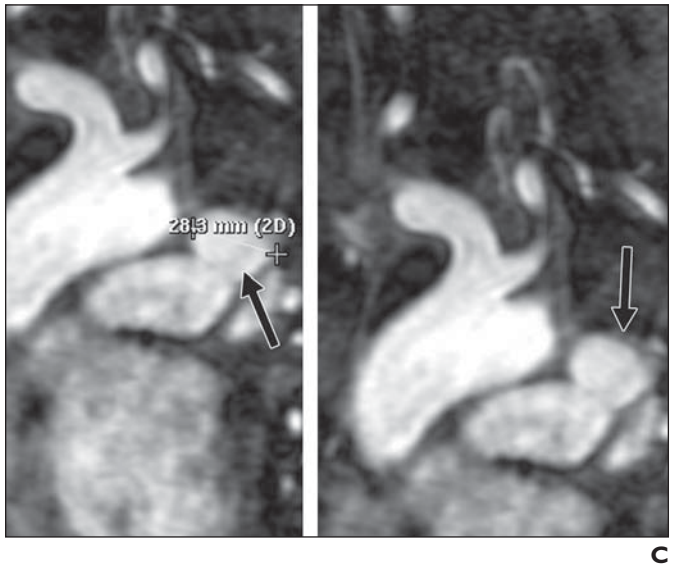

Fig. 21—Aortopulmonary shunts.
A, Line diagram illustrates various surgically created aortopulmonary shunts.
B, Coronal MR angiography image of 21-year-old man after surgical repair of tetralogy of Fallot shows absence of right subclavian artery (*arrowheads*), which was taken down for Blalock-Taussig shunt. Note normal left subclavian artery (*arrow*).
C, MR angiography image in 23-year-old man with history of Tetralogy of Fallot shows pseudoaneurysm (*arrow*) in the distal anastomosis of Blalock-Taussig shunt.

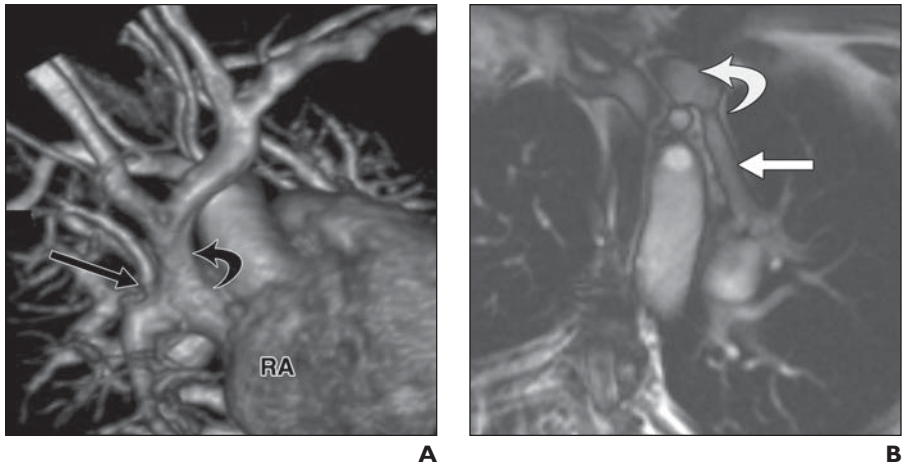

Fig. 22—Partial anomalous pulmonary venous return.
A, Three-dimensional volume-rendered image of 28-year-old woman shows anomalous drainage of right superior pulmonary vein (*straight arrow*) into superior vena cava (*curved arrow*). RA = right atrium.
B, Axial steady-state free precession image of 43-year-old woman shows vertical vein (*straight arrow*) that drains left upper lobe into left brachiocephalic vein (*curved arrow*).

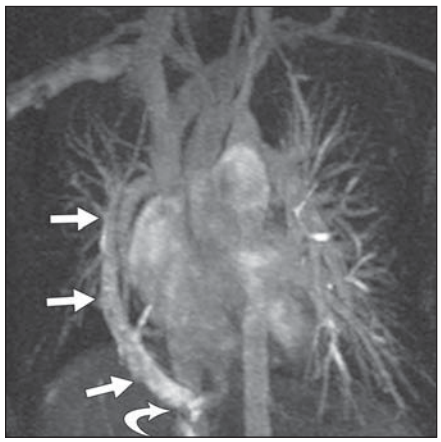

Fig. 23—Scimitar syndrome. Coronal maximum-intensity-projection image of 11-year-old boy shows large anomalous vein (*straight arrows*) shaped like scimitar draining right upper and middle lobes to inferior vena cava (*curved arrow*).

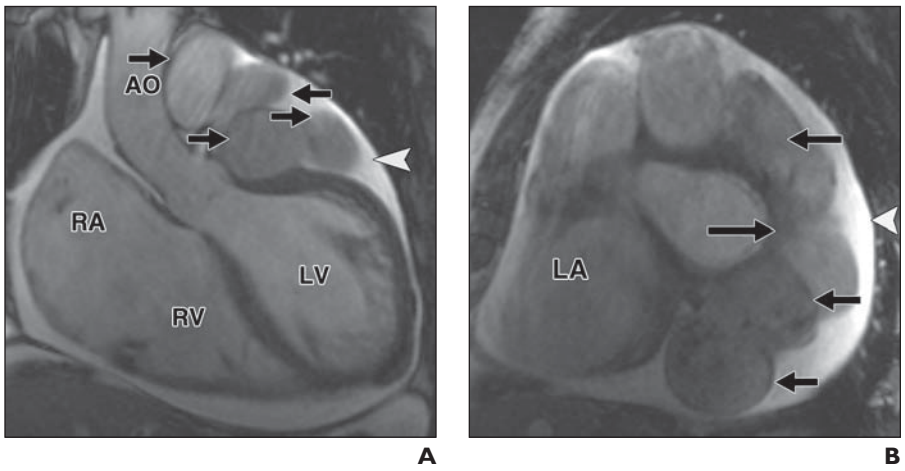

Fig. 24—Coronary artery–coronary sinus fistula in 58-year-old woman.
A, Coronal steady-state free precession (SSFP) image shows severely dilated coronary arteries (*arrows*). There is also small pericardial effusion (*arrowhead*). AO = aorta, RA = right atrium, RV = right ventricle, LV = left ventricle.
B, Sagittal SSFP image shows dilated coronary arteries (*arrows*), which open into right atrium (not shown), and pericardial effusion (*arrowhead*). LA = left atrium

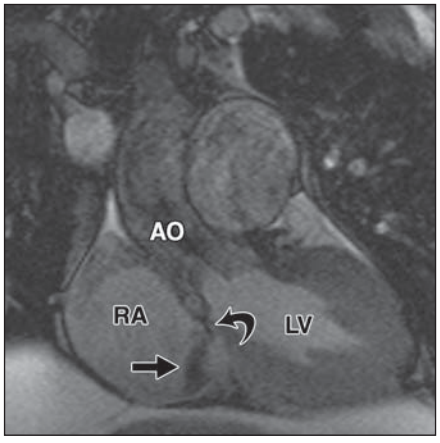

Fig. 25—Aorta-to–right atrium fistula. Coronal oblique steady-state free precession image of 47-year-old man after aortic valve replacement shows communication between aortic root and right atrium (*curved arrow*) with dark jet extending into right atrium (*straight arrow*); these findings are consistent with fistulous communication. AO = aorta, RA = right atrium, LV = left ventricle.

FOR YOUR INFORMATION

The data supplement accompanying this Web exclusive article can be viewed from the information box in the upper right corner of the article at: www.ajronline.org.

FOR YOUR INFORMATION

The reader's attention is directed to part 2 accompanying this article, titled "Cardiac MRI: Part 2, Pericardial Diseases" which begins on page W621.

FOR YOUR INFORMATION

The Self-Assessment Module accompanying this article can be accessed via www.ajronline.org at the article link labeled "CME/SAM."

The American Roentgen Ray Society is pleased to present these Self-Assessment Modules (SAMs) as part of its commitment to lifelong learning for radiologists. Each SAM is composed of two journal articles along with questions, solutions, and references, which can be found online. Read each article, then answer the accompanying questions and review the solutions online. After submitting your responses, you'll receive immediate feedback and benchmarking data to enable you to assess your results against your peers.

Continuing medical education (CME) and SAM credits are available in each issue of the *AJR* and are ***free to ARRS members. Not a member?*** Call 1-866-940-2777 (from the U.S. or Canada) or 703-729-3353 to speak to an ARRS membership specialist and begin enjoying the benefits of ARRS membership today!